

## Analysis of a ray-tracing model for gravity waves generated by tropospheric convection

Dave Broutman<sup>1</sup> and Stephen D. Eckermann<sup>2</sup>

Received 4 October 2011; revised 3 January 2012; accepted 26 January 2012; published 14 March 2012.

[1] The Vadas-Fritts ray-tracing model for convectively generated gravity waves is analyzed using the stationary phase approximation and is interpreted in terms of a ray Jacobian approximated by the density of rays. The Vadas-Fritts model launches rays from the convective source region, with initial conditions for the ray-tracing deduced from a near-field integral representation. In the far-field the rays are binned in space-time grid cells. The contribution of each ray to the spatial wave amplitude is determined by its spectral amplitude and by the local density of rays within the grid cells. The present analysis accomplishes two things. First, the stationary phase analysis gives the formal initial conditions for the ray-tracing, which mostly agree with the Vadas-Fritts initialization but also suggest some refinements. Secondly, the Jacobian and ray-density analysis shows how the Vadas-Fritts model can be generalized to follow a beam of rays with a single moving grid cell.

**Citation:** Broutman, D., and S. D. Eckermann (2012), Analysis of a ray-tracing model for gravity waves generated by tropospheric convection., *J. Geophys. Res.*, 117, D05132, doi:10.1029/2011JD016975.

### 1. Introduction

[2] Gravity waves generated by tropospheric convection can propagate high into the atmosphere, reaching altitudes of 200 kilometers or more. While high resolution simulations using fully nonlinear mesoscale atmospheric models can capture the processes near the tropospheric source, extending these models with sufficient resolution to such high altitudes is computationally impractical. Thus, alternative approaches are required to model the deep penetration of convectively generated gravity waves into the middle and upper atmosphere.

[3] One such approach for convectively generated gravity waves has been developed by *Vadas and Fritts* [2001, 2004, 2005, 2009] and has been used to interpret a number of observations, including airglow data from the mesopause region near 85 km altitude [*Vadas et al.*, 2009] and ionospheric soundings of the F-layer near 250 km altitude [*Vadas and Crowley*, 2010].

[4] The Vadas-Fritts model consists of a Fourier-Laplace integral representation for the near-field around the convective forcing, and a ray-tracing for the propagation of the gravity waves into the far-field. The initial conditions for the far-field ray-tracing are deduced from the near-field integral representation.

[5] In this paper, we examine the Vadas-Fritts ray-tracing model. Our main analysis tool is the stationary phase approximation for the near-field integral representation,

which we present based on the theory of *Lighthill* [1996]. The stationary phase approximation, like the Vadas-Fritts theory, takes spectral wave amplitudes from the near-field integral representation and produces a ray solution for the gravity waves emerging from the forcing. It thus provides all the information necessary to initialize a far-field ray-tracing. Mostly, the stationary phase theory supports the Vadas-Fritts ray-tracing initialization, but there are some small differences that suggest potential refinements to the specification of the initial conditions.

[6] We also examine the Vadas-Fritts method of computing the spatial wave amplitudes in the ray-tracing. Their method is new, at least in the context of gravity waves, in the way that it accounts for the three dimensional geometrical spreading of the rays. In principle, the effects of geometrical spreading on wave amplitudes can be obtained by advecting a ray-tube volume element along each ray, but this is notoriously difficult in practice, as discussed by *Hasha et al.* [2008]. The Vadas-Fritts method is a practical alternative to the ray-tube method and is potentially useful for other gravity wave applications. We analyze the Vadas-Fritts method in a different but equivalent way to their formulation, making explicit use of a ray Jacobian and relating the ray Jacobian to the density of the rays. The advantages of this approach are summarized at the conclusion of the paper.

[7] The paper is organized as follows. In section 2 the Vadas-Fritts model equations are presented, along with an integral representation for the solution. This is followed in section 3 by a presentation of the stationary phase approximation for the integral representation. In section 4 the ray Jacobian and density of rays are discussed in relation to the Vadas-Fritts method of wave amplitude calculation. In section 5 the specific forms for the convective forcing terms of the Vadas-Fritts model are introduced, and examples of

<sup>1</sup>Computational Physics, Inc., Springfield, Virginia, USA.

<sup>2</sup>Space Science Division, Naval Research Laboratory, Washington, D. C., USA.

the solution are presented based on the stationary phase analysis. In section 6 the stationary phase and Vadas-Fritts ray initializations are compared. In section 7, the extension to a non-uniform background is discussed. In section 8 our main results are summarized, with suggestions for further analysis.

[8] We assume a uniform background throughout this paper, except to indicate in section 7 how the method can be extended to a non-uniform background. We also make the Boussinesq approximation and ignore dissipation. While dissipative effects are an important component of the Vadas-Fritts ray-tracing model, they are not needed for our purposes and so are omitted. The presentation is fairly general until section 5, where the specific Vadas-Fritts forcing terms are introduced.

[9] We give a modified derivation of the Vadas-Fritts integral representation using a Fourier transform in time, rather than the Laplace transform of the Vadas-Fritts theory. The modified derivation is based on work by *Lighthill* [1996], and its equivalence to the Vadas-Fritts solution is shown in Appendix A.

## 2. The Vadas-Fritts Model

[10] We consider a simplified form of the Vadas-Fritts model, as used in section 2.1.1 of *Vadas and Fritts* [2009]. It is Boussinesq, incompressible, inviscid, and without the influence of the earth's rotation. The background is uniform and at rest. The linearized governing equations are [see *Vadas and Fritts*, 2001, equation (2)]

$$u_t + p_x/\bar{\rho} = 0, \quad (1)$$

$$v_t + p_y/\bar{\rho} = 0, \quad (2)$$

$$w_t + p_z/\bar{\rho} - g\theta/\bar{\theta} = q(\mathbf{x})r(t), \quad (3)$$

$$\theta_t + \bar{\theta}N^2w/g = 0, \quad (4)$$

$$u_x + v_y + w_z = 0. \quad (5)$$

Here  $t$  is time,  $(u, v, w)$  are the perturbation velocity components in  $\mathbf{x} = (x, y, z)$ , with  $z$  positive upwards,  $N$  is the unperturbed buoyancy frequency,  $g = 9.8 \text{ m s}^{-2}$  is gravitational acceleration,  $p$  and  $\theta$  are the perturbation pressure and potential temperature, and  $\bar{\theta}$  and  $\bar{\rho}$  are the mean potential temperature and density.

[11] The forcing term in (3) has the separable form  $q(\mathbf{x})r(t)$  and is localized in space and time. As in the Vadas-Fritts calculations, we find solutions that are valid for times after the forcing has finished. The forcing represents a single convective plume. We ignore the contribution from waves that initially propagate downward from the source and are reflected back upward by the ground. Ground reflected waves can be included by adding an image source below the ground. Cases with multiple convective plumes and ground reflection are studied by *Vadas and Fritts* [2009]. Throughout our paper, reference to the Vadas-Fritts model means its simplest version, with the above specifications.

[12] Equations (1)–(5) combine to give

$$\nabla^2 w_{tt} + N^2 \nabla_h^2 w = r_t \nabla_h^2 q, \quad (6)$$

where  $\nabla_h^2 = \partial_x^2 + \partial_y^2$  and  $\nabla^2 = \nabla_h^2 + \partial_z^2$ .

[13] We introduce the Fourier transforms

$$R(\omega) = \frac{1}{2\pi} \int r(t) e^{-i\omega t} dt, \quad (7)$$

$$Q(\mathbf{k}) = \frac{1}{(2\pi)^3} \int q(\mathbf{x}) e^{i\mathbf{k}\cdot\mathbf{x}} d\mathbf{x}, \quad (8)$$

and

$$W(\mathbf{k}, \omega) = \frac{1}{(2\pi)^4} \int \int w(\mathbf{x}, t) e^{i(\mathbf{k}\cdot\mathbf{x} - \omega t)} d\mathbf{x} dt. \quad (9)$$

The frequency is  $\omega$ , and the wave number is  $\mathbf{k} = (k, l, m)$ . The spatial integrals above and the wave number integrals below are all three-dimensional, and all integration limits are  $\pm\infty$ . The inverse Fourier transform of (9) is

$$w(\mathbf{x}, t) = \int \int W(\mathbf{k}, \omega) e^{-i(\mathbf{k}\cdot\mathbf{x} - \omega t)} d\mathbf{k} d\omega. \quad (10)$$

Our Fourier transform notation is the same as in equation (A4) of *Lighthill* [1996] and differs from that of equation (2) of *Vadas and Fritts* [2009] in that they place the  $1/2\pi$  factors in the inverse transform rather than the forward transform.

[14] Taking the Fourier transform of (6) in time and space, and solving for  $W$  gives

$$W(\mathbf{k}, \omega) = -i\omega k_h^2 Q R / B, \quad (11)$$

where

$$B(\mathbf{k}, \omega) = \omega^2 (k_h^2 + m^2) - N^2 k_h^2, \quad (12)$$

with  $k_h^2 = k^2 + l^2$ . The dispersion relation for gravity waves is defined by the relation  $B = 0$ . We let  $\sigma$  denote a frequency that satisfies the dispersion relation, i.e.

$$\sigma^2 = k_h^2 N^2 / (k_h^2 + m^2). \quad (13)$$

We take  $\sigma$  to be positive, so the zeros of  $B$  are at  $\omega = \pm\sigma(\mathbf{k})$ .

[15] We define

$$\bar{Q} \equiv -i\omega k_h^2 Q R, \quad (14)$$

so that, from (11),  $W(\mathbf{k}, \omega) = \bar{Q}/B$ . Then (10) becomes

$$w(\mathbf{x}, t) = \int \int (\bar{Q}/B) e^{-i(\mathbf{k}\cdot\mathbf{x} - \omega t)} d\mathbf{k} d\omega. \quad (15)$$

[16] After the transient forcing has finished, the integral (15) becomes [*Lighthill*, 1996]

$$w(\mathbf{x}, t) = \int \tilde{w}(\mathbf{k}, t) e^{-i\mathbf{k}\cdot\mathbf{x}} d\mathbf{k}. \quad (16)$$

Here

$$\tilde{w}(\mathbf{k}, t) = F(\mathbf{k}) e^{i\sigma t} + G(\mathbf{k}) e^{-i\sigma t}, \quad (17)$$

with

$$F(\mathbf{k}) = 2\pi i \bar{Q}(\mathbf{k}, \sigma) / B_\omega(\mathbf{k}, \sigma), \quad (18)$$

$$= \pi(\sigma^2 / N^2) Q(\mathbf{k}) R(\sigma), \quad (19)$$

$$G(\mathbf{k}) = 2\pi i \bar{Q}(\mathbf{k}, -\sigma) / B_\omega(\mathbf{k}, -\sigma), \quad (20)$$

$$= \pi(\sigma^2 / N^2) Q(\mathbf{k}) R(-\sigma). \quad (21)$$

From (12), we have used  $B_\omega \equiv \partial B / \partial \omega = 2\omega(k_h^2 + m^2)$  to arrive at (19) and (21). The notation is that  $w(\mathbf{x}, t)$  has the spatial Fourier transform  $\tilde{w}(\mathbf{k}, t)$  and the space-time Fourier transform  $W(\mathbf{k}, \omega)$ .

### 3. The Stationary Phase Approximation

[17] The stationary phase solution for (16) derived by *Lighthill* [1996], and designated here by  $w_1$ , is

$$w_1 = (2\pi N t)^{3/2} r^{-3} \sin\theta \cos^{1/2}\theta [F(\mathbf{k})e^{i\alpha} + G(-\mathbf{k})e^{-i\alpha}]. \quad (22)$$

This is expressed in spherical coordinates  $(r, \theta, \phi)$ , where

$$x = r \sin\theta \cos\phi, \quad y = r \sin\theta \sin\phi, \quad z = z_0 + r \cos\theta. \quad (23)$$

The source is centered at  $\mathbf{x}_0 = (0, 0, z_0)$ .

[18] The wave phase in (22) is

$$\alpha = N t \cos\theta + \pi/4 - m z_0, \quad (24)$$

$$= \sigma t + \pi/4 - m z_0. \quad (25)$$

We have used  $\sigma = N \cos\theta$  from (13) and (26) to obtain (25) from (24).

[19] The wave number components are

$$k = K \cos\theta \cos\phi, \quad l = K \cos\theta \sin\phi, \quad m = -K \sin\theta. \quad (26)$$

The wave number magnitude is

$$K = (N t / r) \sin\theta. \quad (27)$$

This is the stationary phase condition. It is equivalent to

$$r = |\mathbf{c}_g| t, \quad (28)$$

since the group velocity vector  $\mathbf{c}_g$  has magnitude  $N |\sin\theta| / K$ .

[20] In the stationary phase solution (22), the position, time, and wave number cannot all be set independently. They are related by the stationary phase condition (27) or (28).

[21] For example, if  $K$  and  $\theta$  are fixed, then according to (28) the position  $r$  moves at speed  $|\mathbf{c}_g| t$ . This is equivalent to following a ray. The stationary phase solution (22) then shows that the wave amplitude decreases along the ray as  $t^{-3/2}$  or as  $r^{-3/2}$ . This decrease is the result of geometrical spreading.

[22] The reason that the wave number argument of  $G$  in (22) has a negative sign is to match the negative sign in the associated wave phase, with frequency  $-\sigma$ . The combination

$-\mathbf{k}, -\sigma$  has the same group velocity and corresponds to the same ray as the combination  $\mathbf{k}, \sigma$ . Nevertheless, these are two linearly independent terms, and both are needed to satisfy arbitrary initial conditions.

### 4. Jacobian Approximation and Ray Density

[23] The stationary phase solution (22) contains the factor

$$J^{-1/2} = (N t)^{3/2} r^{-3} \sin\theta \cos^{1/2}\theta. \quad (29)$$

Here  $J$  is the Jacobian determinant

$$J = |\partial(x, y, z) / \partial(k, l, m)| \quad (30)$$

of the ray transformation between wave number and spatial coordinates. The ray transformation is the stationary phase condition (27) or (28).

[24] The stationary phase solution (22) is expressed in terms of the Jacobian as

$$w_1(\mathbf{x}, t) = (2\pi)^{3/2} J^{-1/2} W_1, \quad (31)$$

where

$$W_1(\mathbf{k}, t) = F(\mathbf{k})e^{i\alpha} + G(-\mathbf{k})e^{-i\alpha}. \quad (32)$$

We refer to  $W_1$  as the spectral stationary phase solution, or the spectral ray solution.

[25] The aim here is to find a practical approximation for the Jacobian  $J$  that can be used in a numerical ray-tracing algorithm to convert spectral wave amplitudes, obtained from the near-field integral representation, to spatial wave amplitudes along the ray. This is done here by considering the density of rays.

[26] We rewrite  $J$  as the ratio of infinitesimal volume elements  $J = d\mathbf{x} / d\mathbf{k}$ . As noted by *Lighthill* [1996, equation (A11)], the spatial volume element of size  $d\mathbf{x} = J d\mathbf{k}$  is occupied by waves with wave number  $\mathbf{k}$  lying in a spectral volume element of size  $d\mathbf{k}$ . The spatial volume element  $d\mathbf{x}$  is carried along the ray and expands in size as  $t^3$ , a result of the geometrical spreading of the waves away from the source. The factor of  $t^3$  is obtained from  $J \sim r^6 / t^3$  in (29) with  $r = |\mathbf{c}_g| t$  along the ray. For a uniform background, the size of the spectral volume element  $d\mathbf{k}$  remains constant following the ray.

[27] Let wave number space be discretized with grid cells of finite volume  $\delta\mathbf{k}$ . Suppose we launch one ray from each wave number grid cell. Then the density of rays in the wave number domain is  $1 / \delta\mathbf{k}$ . The associated density of rays in the spatial domain is  $1 / \delta\mathbf{x}$ , where  $\delta\mathbf{x} \simeq J \delta\mathbf{k}$ . The last expression is approximate because  $J$  is approximated by its value at the center of the wave number grid cell. The finite-sized volume element  $\delta\mathbf{x}$ , like the infinitesimal volume element  $d\mathbf{x}$ , is carried along the ray and expands in size (approximately as  $t^3$ ) due to geometrical spreading. To summarize,

$$\text{spectral ray density} = 1 / \delta\mathbf{k}, \quad (33)$$

$$\text{spatial ray density} = 1 / \delta\mathbf{x} \simeq 1 / (J \delta\mathbf{k}). \quad (34)$$

[28] Next we introduce a fixed spatial grid with grid cells of fixed size  $\Delta \mathbf{x}$ . Let the number of rays in a particular spatial grid cell at time  $t$  be  $n$ . Then in that grid cell,

$$\text{spatial ray density} = 1/\delta \mathbf{x} \simeq n/\Delta \mathbf{x}. \quad (35)$$

Hence (34) and (35) imply that

$$J \simeq \delta \mathbf{x} / \delta \mathbf{k} \simeq (\Delta \mathbf{x} / n) (1 / \delta \mathbf{k}). \quad (36)$$

[29] In ray-tracing, it is usually the squared wave amplitude in some form (e.g. wave action, wave momentum flux), that is advected along the ray. Working with the vertical velocity (until section 7), the squared wave amplitude for  $w_1$  is, from (31) and (36),

$$\langle w_1 w_1^* \rangle = (2\pi)^3 J^{-1} \langle W_1 W_1^* \rangle, \quad (37)$$

$$\simeq (2\pi)^3 (\delta \mathbf{k} / \Delta \mathbf{x}) n \langle W_1 W_1^* \rangle. \quad (38)$$

where  $\langle \rangle$  is an average over the wave phase, the asterisk indicates a complex conjugate, and the value for  $\langle W_1 W_1^* \rangle$  refers to some central ray in the spatial grid cell. Alternatively, the solution can be averaged over each grid cell:

$$\langle w_1 w_1^* \rangle \simeq (2\pi)^3 (\delta \mathbf{k} / \Delta \mathbf{x}) \sum_{j=1}^n \langle W_1 W_1^* \rangle_j. \quad (39)$$

Here  $j$  is an index for each ray.

[30] The steps for the ray-tracing algorithm are then:

[31] 1. Discretize wave number space with elements of size  $\delta \mathbf{k}$ .

[32] 2. Launch one ray for each wave number element.

[33] 3. Assign each ray its spectral wave amplitude  $\langle W_1 W_1^* \rangle$ .

[34] 4. Ray-trace from position  $\mathbf{x}_0$  at time  $t = 0$ .

[35] 5. Bin the rays spatially, in grid cells of size  $\Delta \mathbf{x}$ .

[36] 6. Use (39) to compute the spatial wave amplitude.

This is close to the Vadas-Fritts algorithm. They use somewhat different initial conditions, as we shall discuss in section 6. They also bin the rays in four-dimensional grid cells that are discretized in time as well as in space.

[37] The ray Jacobian appears implicitly in the Vadas-Fritts theory through a normalization factor that is the quotient of the wave number volume element  $\Delta \mathbf{k}$  and the spatial volume element  $\Delta \mathbf{x}$  [Vadas and Fritts, 2009, equation (62)].

[38] Note the distinction between a ray-tube method [Hasha *et al.*, 2008] and the ray-density method (39). The ray-tube method computes geometrical spreading rates explicitly and has to keep track of the varying size of  $\delta \mathbf{x}$  along the ray. Each ray individually provides the spatial wave amplitude on that ray. The ray-density method computes geometrical spreading rates implicitly from the density of rays in a spatial volume element of predetermined size  $\Delta \mathbf{x}$ . Each ray individually provides the spectral wave amplitude along that ray, but many ray-tracings are needed to estimate the spatial wave amplitude from the ray density.

## 5. Vadas-Fritts Forcing

[39] We now set the forcing terms  $q(\mathbf{x})$  and  $r(t)$  in (3), using the same functional form and parameter settings

following Vadas and Fritts [2009]. The spatial dependence  $q(\mathbf{x})$  takes the Gaussian form

$$q = q_0 \exp \left[ - (x^2 + y^2) / L^2 - (z - z_0)^2 / D^2 \right], \quad (40)$$

where  $q_0$ ,  $L$ ,  $D$ , and  $z_0$  are constants.

[40] The temporal dependence  $r(t)$  is

$$r(t) = \frac{1}{\tau} \begin{cases} 1 - \cos at & \text{for } 0 \leq t \leq \tau \\ 0 & \text{otherwise} \end{cases} \quad (41)$$

where  $\tau$  is a constant, and  $a = 2\pi/\tau$ . The Fourier transform (41) of  $r(t)$  is

$$R(\omega) = \frac{a}{\tau} \frac{\text{sinc}(\omega\tau/2)}{a^2 - \omega^2} e^{-i\omega\tau/2}. \quad (42)$$

[41] The buoyancy frequency  $N = 0.02 \text{ s}^{-1}$ . The forcing scales are, spatially,  $L = 20/4.5 \text{ km}$ ,  $D = 10/4.5 \text{ km}$ , and temporally,  $\tau = 12 \text{ min}$ . The forcing is centered at  $z_0 = 7 \text{ km}$ . We set the arbitrary forcing magnitude  $q_0 = 10^3 \text{ ms}^{-1}$  because this value conveniently gives  $O(1)$  perturbation velocities (in  $\text{ms}^{-1}$ ) over much of the spatial domain of interest. The value for  $q_0$  may seem large, but see the comments of Vadas and Fritts [2004, p. 788] about how the forcing is largely balanced by pressure and potential temperature perturbations rather than by large vertical motions.

[42] Since the forcing functions  $r(t)$  and  $q(\mathbf{x})$  are real, their Fourier transforms satisfy  $R(\omega) = R^*(-\omega)$  and  $Q(\mathbf{k}) = Q^*(-\mathbf{k})$ , where the asterisk denotes a complex conjugate. Hence from (19) and (21),

$$F^*(\mathbf{k}) = G(-\mathbf{k}). \quad (43)$$

We write  $F = |F| \exp(i\beta)$ . From (19), the complex argument  $\beta$  of  $F$  is equal to the sum of the complex arguments of  $Q$  and  $R$ . These arguments are, respectively,

$$\beta_Q = m z_0, \quad (44)$$

$$\beta_R = -\sigma\tau/2 + \arg[\sin(\sigma\tau/2)/(a - \sigma)]. \quad (45)$$

Since the term in square parentheses in (45) is real, the argument function in (45) is either zero or  $\pi$ , depending on whether the sign of that term is positive or negative, respectively. Since  $a$  and  $\sigma$  are positive, we can write  $a - \sigma$  instead of  $a^2 - \sigma^2$  in (45).

[43] The spectral ray solution  $W_1$  is then, starting with (32) and taking  $\alpha$  from (25),

$$W_1(\mathbf{k}, t) = F(\mathbf{k}) e^{i\alpha} + G(-\mathbf{k}) e^{-i\alpha}, \quad (46)$$

$$= 2|F(\mathbf{k})| \cos(\sigma t + \pi/4 - m z_0 + \beta), \quad (47)$$

$$= 2|F(\mathbf{k})| \cos(\sigma t + \pi/4 + \beta_R). \quad (48)$$

The stationary phase solution (31) becomes

$$w_1(\mathbf{x}, t) = (2\pi)^{3/2} J^{-1/2} 2|F(\mathbf{k})| \cos(\sigma t + \pi/4 + \beta_R). \quad (49)$$

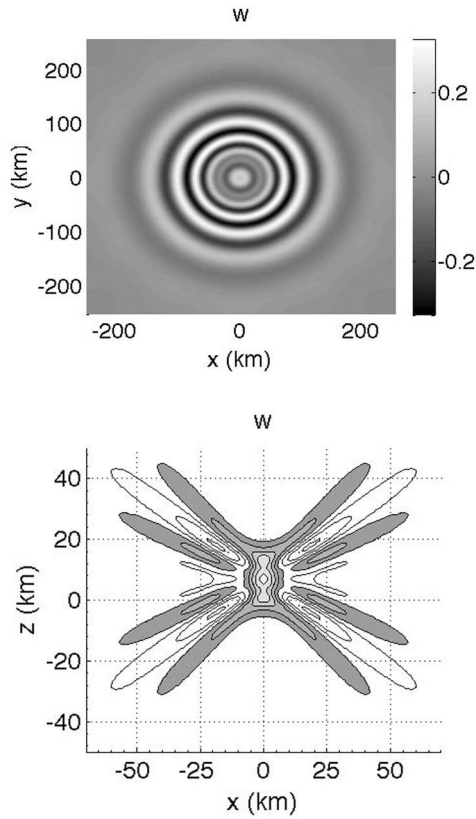


**Figure 1.** The vertical velocity  $w$  derived from the exact integral solution (16) without stationary phase approximation. (top) Horizontal cross section at  $z = 70$  km and  $t = 45$  min. Range (see color bar) is  $\pm 0.33 \text{ ms}^{-1}$ . (bottom) Vertical cross section at  $y = 0$  and  $t = 20$  min, with contour levels of  $\pm(0.1, 0.3, 0.5, 0.7, 0.9)$  times the maximum  $w$  of  $3.7 \text{ ms}^{-1}$ . Positive values are shaded.

The spectral amplitude  $F(\mathbf{k})$ , defined generally in (19), becomes

$$F(\mathbf{k}) = \frac{a^2 \sigma Q}{\tau N^2 (a^2 - \sigma^2)} \quad (50)$$

with magnitude

$$|F(\mathbf{k})| = \frac{a^2 \sigma |Q|}{\tau N^2 |a^2 - \sigma^2|} |\sin(\sigma\tau/2)|. \quad (51)$$

[44] Figure 1 shows solutions calculated from the exact integral (16). Figure 1 (top) plots  $w$  at  $z = 70$  km and  $t = 45$  min. This corresponds to the third row of Figure 6 of *Vadas and Fritts* [2009], but without ground reflection. Figure 1 (bottom) is a vertical cross section of  $w$  for the case without ground reflection in Figure 1c of *Vadas and Fritts* [2009], and is plotted here using their same contour values. These calculations were made with a discrete Fourier transform approximation to the Fourier integral (16), on a spatial grid of (128, 128, 192) points in  $x, y, z$ , respectively. The grid spacing is 4 km in the horizontal directions, and 2.33 km in the vertical.

[45] Figure 2 compares the exact integral solution (16) for  $w$  and its stationary phase approximation  $w_1$  in (49). The comparison is at  $t = 30$  min and at three heights of 30, 40, and 50 km. The solutions are symmetric about the  $x$  axis. The stationary phase solution  $w_1$  is zero along the vertical axis at  $x = 0$  because no rays reach these points. The rays that are directed vertically upward from the source have  $\sigma = N$  and hence zero group velocity.

[46] We now consider the ray-density method for computing wave amplitudes. The idea is to compute the spatial solution  $w_1$  in (49) from a ray-density approximation for the Jacobian  $J$ . From (48),

$$\langle W_1 W_1^* \rangle = 2|F|^2. \quad (52)$$

Using this, (39) becomes

$$\langle w_1 w_1^* \rangle \simeq (2\pi)^3 2(\delta\mathbf{k}/\Delta\mathbf{x}) \sum_{j=1}^n |F(\mathbf{k})|_j^2. \quad (53)$$

The ray-density approximation for  $w_1$  in (49) is then

$$w_1 \simeq \langle w_1 w_1^* \rangle^{1/2} \cos(\sigma t + \pi/4 + \beta_R). \quad (54)$$

[47] In the Vadas-Fritts calculation the spatial grid cells of size  $\Delta\mathbf{x}$  are fixed in space, but they can also move to follow a group of rays. We show two examples, one with a moving spatial grid cell and one with a fixed spatial grid cell. Both cases have the same spatial grid cell volume  $\Delta\mathbf{x}$  and dimensions 4 km by 4 km by 2.33 km, in  $x, y$ , and  $z$ , respectively. This is the same spatial grid size used in the calculation of Figure 1. The solutions are calculated every 0.75 min from  $t = 25$  min to  $t = 59.5$  min and plotted as a function of  $t$ .

[48] The wave number grid cell is centered at  $(k_0, 0, m_0)$  and has 21 wave numbers in each of the three components for a total of  $21^3 = 9261$  launched rays. The central wave

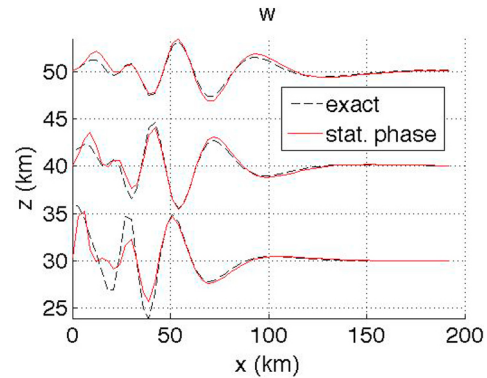


**Figure 2.** The vertical velocity  $w$  along the positive  $x$  axis, at  $t = 30$  min and at three heights, 30, 40, and 50 km. The solutions are computed from the stationary phase approximation (solid) and the exact integral (dashed). The  $w$  solution at each comparison height is plotted using that height as the  $y$ -axis origin. Maximum values for the stationary phase solution in  $\text{ms}^{-1}$  are 0.89, 0.68 and 0.59 at heights 30, 40, and 50 km, respectively.

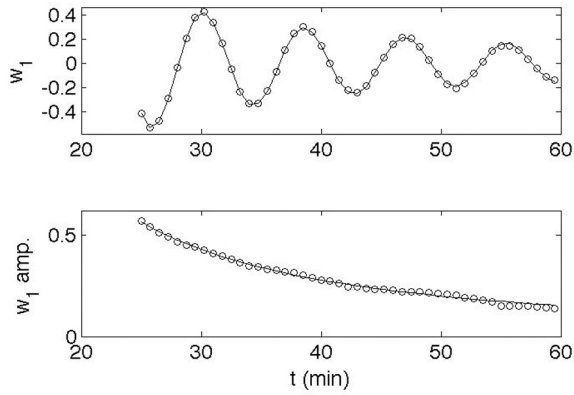


**Figure 3.** An illustration of the ray density method for one grid cell following a group of rays. Solid curves denote the analytic stationary phase solution for (top)  $w_1$  and (bottom) its peak amplitude. The units for  $w_1$  in both panels are  $\text{ms}^{-1}$ . Circles denote the solution from the ray-density method.

number corresponds to a horizontal wavelength of 24.3 km, a vertical wavelength of 19.3 km, an intrinsic frequency of  $\sigma = 0.6N$ , and a group velocity that reaches  $\mathbf{x} = (80, 0, 70)$  km at  $t \approx 45$  min. The wave number grid cell size is  $\delta\mathbf{k} = \delta k \delta l \delta m$  with  $\delta k = 1.72$ ,  $\delta l = 1.83$ , and  $\delta m = 3.28$ , each in units of  $10^{-6} \text{m}^{-1}$ .

[49] In Figure 3, we compare solutions for the case of a moving spatial grid cell. The solid curves denote the stationary phase solution (49) for  $w_1$  (Figure 3, top) and its peak amplitude (Figure 3, bottom). The circles denote the corresponding values obtained from the ray-density method using (54) for Figure 3 (top) and (53) for Figure 3 (bottom). The wave phase in (54) is evaluated along the ray using the central wave number noted above. The center of the spatial grid cell moves from about  $\mathbf{x} = (44, 0, 42)$  km at  $t = 25$  min to about  $\mathbf{x} = (105, 0, 91)$  km by  $t = 60$  min. Recall that the source is centered at  $\mathbf{x}_0 = (0, 0, 7)$  km.

[50] The theoretical stationary-phase prediction for the number of rays contained in the moving spatial grid cell is

$$n \approx \Delta\mathbf{x}/(J\delta\mathbf{k}) \quad (55)$$

$$= (\Delta\mathbf{x}/\delta\mathbf{k})(Nt)^3 r^{-6} \sin^2\theta \cos\theta. \quad (56)$$

Here we have used (36) and the expression for  $J$  in (29). Relative to the source, the center of the spatial grid cell is located at a fixed angle  $\theta = \cos^{-1}(\sigma/N)$  of about  $53^\circ$  from the vertical.

[51] Figure 4 shows the number of rays in the grid cell predicted theoretically (solid curve) by (56) and the number of rays counted in the ray-tracing calculation (circles).

[52] Figure 5 shows the solutions when the grid cell remains at a fixed location centered around the point  $x = 80$  km,  $y = 0$ ,  $z = 70$  km. The solid curves denote the stationary phase solution (49) for  $w_1$  (Figure 5, top) and its peak amplitude (Figure 5, bottom). The stationary phase amplitude grows until about 42 min and then decreases. The circles denote the corresponding solution from the ray-density method using (54) in Figure 5 (top) and (53) in

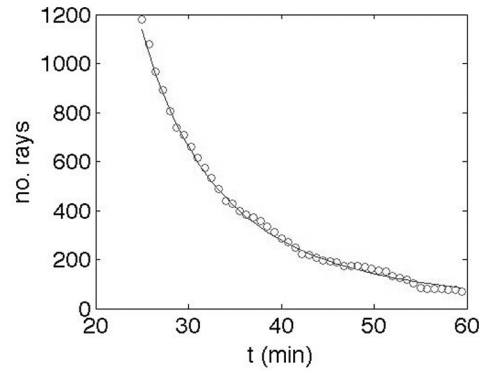


**Figure 4.** The number of rays in the moving spatial grid cell of Figure 3. The solid curve is the number predicted by the stationary phase solution (56). Circles denote the number of rays counted in the numerical ray-tracing.

Figure 5 (bottom). Because we are considering a limited wave number range in the ray-tracing, with a bandwidth in wave number magnitude  $\delta K/K \approx 0.17$ , the grid cell contains rays for only a short time. No rays propagate into the grid cell until  $t \approx 41$  min, and none are left in the grid cell after  $t \approx 49$  min. This time range, and the associated bandwidth for  $K$ , are consistent with the stationary phase condition (27).

## 6. Initialization of the Ray-Tracing

[53] We now compare the ray initialization obtained from stationary phase with the ray initialization implemented in the Vadas-Fritts model. Vadas-Fritts advect along each ray a spectral wave-momentum flux. We can most readily explain the differences between the Vadas-Fritts and stationary phase initializations by working instead with the spectral vertical velocity, as in previous sections. We consider spectral amplitudes more generally in section 7.

### 6.1. Stationary Phase Initialization

[54] The stationary phase condition (28) shows that all rays are launched from  $\mathbf{x}_0 = (0, 0, z_0)$  at  $t = 0$ . The initial

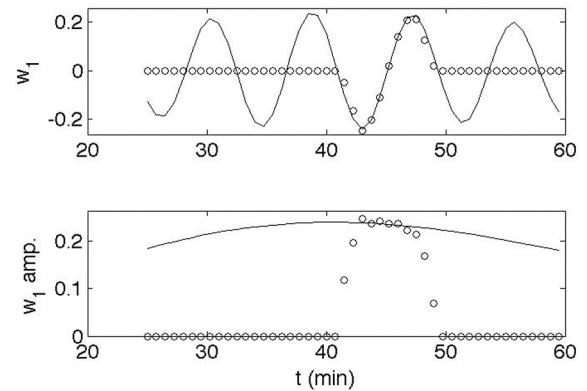


**Figure 5.** Same as Figure 3 but for a grid cell at a fixed location. Solid curves denote the stationary phase solution. Circles denote the ray-density method.

wave phase is  $\pi/4 + \beta_R$ , as indicated by (48). The mean square spectral wave amplitude for the ray-tracing is  $2|F|^2$ , as also indicated by (48). As noted in the discussion preceding (19), our solution for  $F$  is valid for times  $t > \tau$ , after the forcing vanishes. We can still use this  $F$  to initialize the ray-tracing, but the solution is not valid until  $t > \tau$ .

[55] In summary, the ray-tracing initial conditions from stationary phase are:

$$\text{time} = 0, \quad (57)$$

$$\text{position} = \mathbf{x}_0, \quad (58)$$

$$\text{wave phase} = \pi/4 + \beta_R, \quad (59)$$

$$\text{mean squared wave amplitude} = \langle W_1 W_1^* \rangle, \quad (60)$$

$$= 2|F|^2, \quad (61)$$

with  $|F|$  given by (51) and  $\beta_R$  by (45).

## 6.2. Vadas-Fritts Initialization

[56] Vadas-Fritts initialize their ray-tracing with a spectral amplitude derived from an integral representation involving a Laplace transform in time. In Appendix A, we demonstrate that their result can be reproduced using the Fourier transform approach developed in earlier sections, giving an equivalent  $\tilde{w}(\mathbf{k}, t)$  in (A7). The spectral amplitude for times  $t > \tau$ , after the forcing stops, is

$$|\tilde{w}(\mathbf{k}, t > \tau)| = 2 \frac{a^2 \sigma |Q|}{\tau N^2 |a^2 - \sigma^2|} |\sin(\sigma\tau/2)|. \quad (62)$$

This is equivalent to the spectral amplitude  $2|F|$  in the stationary phase solution (49), with  $|F|$  given by (51). Vadas-Fritts account for any additional constant factors, such as the  $(2\pi)^{3/2}$  in the stationary phase solution, through their normalization, which is done by comparing the ray solution with the exact integral solution [Vadas and Fritts, 2009, p. 162].

[57] The wave phase in the Vadas-Fritts model is given by [Vadas and Fritts, 2009, equation (46)]

$$\phi_{vf}(t) = \phi_0 + \int_{t_i}^t \sigma dt. \quad (63)$$

The rays are launched at time  $t_i$  from position  $\mathbf{x}_0$  with initial phase  $\phi_0$ . The sign before the integral in (63) is negative in the Vadas-Fritts notation but positive here. The integral is taken along the ray and reduces to  $\sigma(t - t_i)$  for a uniform background.

[58] Vadas-Fritts choose  $\phi_0$  to be the wave phase at  $t = \tau$ . This is a natural choice, given that the wave phase contains the phase of  $\tilde{w}$  in (A7), and this solution for  $\tilde{w}$  is not valid until  $t = \tau$ . Vadas-Fritts then adjust the launch time of the rays to find the best ray approximation to the exact integral solution, settling on  $t_i = \tau/2$  [Vadas and Fritts, 2009, p. 161].

[59] For the Vadas-Fritts choice of  $\phi_0$ , the stationary phase solution indicates that the rays should be launched at  $t_i = \tau$

from the ray-dependent position  $\mathbf{x}_0 + \mathbf{c}_g \tau$ , where  $\mathbf{c}_g$  is the group velocity vector of the ray. This is consistent with the stationary phase prediction that all rays originate from  $\mathbf{x}_0$  at  $t = 0$ . Alternatively, one can simply launch all rays from  $\mathbf{x}_0$  at  $t = 0$  with  $\phi_0$  set to the wave phase at  $t = 0$ , as in section 6.1. Although  $\phi_0$  contains the phase of  $\tilde{w}$  in (A7), which is not correct until  $t = \tau$ , this initialization will give the correct stationary phase solution for times  $t > \tau$ .

[60] The Vadas-Fritts initialization of the wave phase omits the  $\pi/4$  phase shift in the stationary phase solution (49). Our calculations indicate that this has a relatively small effect on the solution for the Vadas-Fritts parameters.

## 7. Extension to a Non-uniform Background

[61] Consider the relation [cf. Bühler *et al.*, 1999, equation (19)]

$$\int_{\mathcal{D}(t)} \langle ss^* \rangle d\mathbf{x} = (2\pi)^3 \int_{\mathcal{K}(t)} \langle SS^* \rangle d\mathbf{k}. \quad (64)$$

Here  $s(\mathbf{x}, t)$  is the ray solution for any field variable, and  $S(\mathbf{k}, t)$  is the corresponding ray variable in Fourier space. For the previous results  $s = w_1$  of (22) and (31), and  $S = W_1$  of (32). The regions  $\mathcal{D}(t)$  and  $\mathcal{K}(t)$  are related point-wise by the group velocity condition, which for a non-uniform background is  $\mathbf{x} = \int \mathbf{c}_g dt$ , with the integral taken along the ray.

[62] For sufficiently small volumes, (64) approximates to

$$\langle ss^* \rangle = (2\pi)^3 \langle SS^* \rangle \delta\mathbf{k} / \delta\mathbf{x}, \quad (65)$$

where the finite volume elements  $\delta\mathbf{x}$  and  $\delta\mathbf{k}$  introduced in section 4 correspond to  $\mathcal{D}(t)$  and  $\mathcal{K}(t)$ , respectively.

[63] For a uniform background,  $\langle SS^* \rangle$  and  $\delta\mathbf{k}$  are constant along the ray, and  $\delta\mathbf{x}$  can be estimated by the ray density method, as in (35).

[64] For a non-uniform background,  $\langle SS^* \rangle$  and  $\delta\mathbf{k}$  both vary following the ray, but if  $\langle SS^* \rangle$  represents a conserved quantity, such as the wave-action density, then by definition the product of  $\langle SS^* \rangle$  and  $\delta\mathbf{k}$  is constant following the ray during conservative propagation. Using the ray-density approximation  $\delta\mathbf{x} = \Delta\mathbf{x}/n$ , as in (35), we obtain

$$\langle ss^* \rangle = (2\pi)^3 \langle SS^* \rangle_0 \delta\mathbf{k}_0 n / \Delta\mathbf{x}. \quad (66)$$

The zero subscript above indicates an initial value, for example at  $t = \tau$  in (41) when the forcing has just finished. We have assumed that one ray is launched from each wave number volume element of size  $\delta\mathbf{k}_0$ . Equation (66) is the generalization of (38) for a non-uniform background.

[65] Another way of deriving (66) is through the conservation equation for wave action in the form given by Hayes [1970]:

$$AJ_H = \text{constant along a ray}. \quad (67)$$

Here  $A$  is the wave-action density per unit volume, and  $J_H$  is the Jacobian of the Hayes formulation:

$$J_H = |\partial(x, y, z) / \partial(a, b, c)|. \quad (68)$$

The vector  $\mathbf{a} = (a, b, c)$  is a label for each ray. To conform with Vadas-Fritts, we choose  $\mathbf{a} = \mathbf{k}_0$ , the initial wave number of the ray. Then

$$AJ_H \approx A\delta\mathbf{x}/\delta\mathbf{k}_0 \quad (69)$$

$$\approx [A\delta\mathbf{x}/\delta\mathbf{k}_0]_{\mathbf{x}\rightarrow\mathbf{x}_0} \quad (70)$$

$$\approx \tilde{A}_0, \quad (71)$$

where  $\tilde{A}_0$  is the spectral wave-action density at  $\mathbf{x}_0$ .

[66] Using, as in (35), the ray-density approximation  $\delta\mathbf{x} \approx \Delta\mathbf{x}/n$  with (69) and (71) gives

$$A = \tilde{A}_0 \delta\mathbf{k}_0 n/\Delta\mathbf{x}. \quad (72)$$

This is equivalent to (66) with  $A = \langle SS^* \rangle$  and  $\tilde{A}_0 = (2\pi)^3 \langle SS^* \rangle_0$ .

[67] The integral ray formulation (64) and the Hayes ray formulation (67) are completely general in that the background can vary in all directions and in time, and the wavefield can be transient or steady state. Thus the corresponding ray-density approximations (66) and (72) are also general. It is only necessary to assume a uniform background for the near-field Fourier analysis, which determines the initial condition for (64) and the constant in (67).

## 8. Summary and Outlook

[68] We used the stationary phase method to analyze the Vadas-Fritts ray-tracing model of gravity waves generated by a convective plume. Like Vadas-Fritts, stationary phase takes spectral wave amplitudes from a near-field integral representation and converts them to spatial wave amplitudes along raypaths. It provides all quantities necessary to initialize a ray-tracing, as we discussed in section 6. It also expresses the conversion factor from spectral to spatial wave amplitudes in terms of a ray Jacobian. As discussed in section 4, the Vadas-Fritts method in essence uses the density of rays to approximate the ray Jacobian, and the ray Jacobian to convert spectral wave amplitudes to spatial wave amplitudes.

[69] Introducing the ray Jacobian explicitly is beneficial in three ways. First, the ray Jacobian is useful in itself for estimating geometrical spreading rates, which affect local wave amplitudes. While the analytic expression for the ray Jacobian in (29) is valid for a uniform background, this is sometimes sufficient for rough estimates of geometrical spreading rates in more general backgrounds, as in Table 1 of *Fritts and Vadas* [2008]. The present analysis suggests that this Fritts-Vadas estimate can be improved. They assume that the gravity wave momentum flux is proportional to  $r^{-2}$  following a ray, where  $r$  is the distance from the source. This takes into account geometrical spreading in the horizontal directions, but the geometrical spreading is three dimensional for a transient source of gravity waves. The wave amplitude is then proportional to  $r^{-3/2}$ , as noted at the end of section 3, and the momentum flux is proportional to  $r^{-3}$ .

[70] Secondly, the accuracy of the Vadas-Fritts conversion of spectral to spatial wave amplitudes along the ray is equivalent to the accuracy of the ray-density approximation for the ray Jacobian. Thus the ray Jacobian approximation

alone can be analyzed and tested in order to estimate the number of rays needed for accurate wave amplitude calculation in a specific application.

[71] Third, the ray Jacobian identifies the conversion of spectral to spatial wave amplitudes as a local transformation. Thus the Vadas-Fritts method can be applied locally to follow a beam of rays, with a single moving grid cell rather than a three dimensional spatial grid of many stationary cells. We showed an example in Figure 3. The moving grid cell may be a useful generalization of the Vadas-Fritts method.

[72] We limited our analysis to the simplest case of a uniform windless background, except for the derivation in section 7 that indicates how to extend the method to a non-uniform background. For further tests and analysis, the Vadas-Fritts method could be compared with the exact integral solution and stationary phase approximation of *Shutts* [1998] for mountain waves in wind shear, and of *Dupont and Voisin* [1996] for gravity waves generated by a translating oscillating source in a uniform background. Both of these models have regions of strong ray focusing where standard ray methods break down, including caustics. The ray density method has the potential to smooth out caustics and related focusing regions and produce more accurate estimates of the wave amplitudes than obtained from standard spatial ray-tracing methods. The ability of the ray-density method to smooth out caustics has been demonstrated in a case of electromagnetic waves by *Didascalou et al.* [2000].

## Appendix A

[73] We used a Fourier transform in time for the near-field integral representation in (9) and (10) rather than the Laplace transform in time of the Vadas-Fritts theory. We check that our result matches Vadas-Fritts, i.e. that the inverse Fourier transform

$$\tilde{w}(\mathbf{k}, t) = \int W(\mathbf{k}, \omega) e^{i\omega t} d\omega \quad (A1)$$

gives the same  $\tilde{w}(\mathbf{k}, t)$  as *Vadas and Fritts* [2009, equation (12)] obtained by inverse Laplace transform. Here  $W(\mathbf{k}, \omega)$  is defined in (9) as the space-time Fourier transform of the vertical velocity  $w$ .

[74] We substitute for  $W(\mathbf{k}, \omega)$  from (11) and displace the integration path in (A1) by  $-i\epsilon$  to obtain

$$\tilde{w}(\mathbf{k}, t) = -ik_h^2 Q \int_{-i\epsilon-\infty}^{-i\epsilon+\infty} (\omega R/B) e^{i\omega t} d\omega. \quad (A2)$$

The small positive  $\epsilon$  will ultimately tend to zero. As noted by *Lighthill* [1996, 1978, p. 267], the introduction of  $\epsilon$  ensures that the system is completely undisturbed in the limit of large negative  $t$ . See also the causality comments by *Voisin* [2003, equation (2.16)].

[75] From the integrand of (A2) and  $R(\omega)$  in (42) we have

$$\omega R e^{i\omega t} = \frac{2a}{\tau^2} \frac{\sin(\omega\tau/2)}{a^2 - \omega^2} e^{i\omega(t-\tau/2)}, \quad (A3)$$

$$= -\frac{ia}{\tau^2} \frac{1}{a^2 - \omega^2} [e^{i\omega t} - e^{i\omega(t-\tau)}]. \quad (A4)$$

Substituting (A4) into (A2) leaves

$$\tilde{w}(\mathbf{k}, t) = \frac{-k_h^2 a Q}{\tau^2} \int_{-i\epsilon - \infty}^{-i\epsilon + \infty} \frac{e^{i\omega t} - e^{i\omega(t-\tau)}}{(a^2 - \omega^2)B} d\omega, \quad (\text{A5})$$

The poles of this integrand are at  $B = 0$  (not  $\omega = \pm a$ ) and correspond to the frequencies that satisfy the dispersion relation  $\omega = \pm \sigma(\mathbf{k})$ .

[76] For  $t < 0$ , before the forcing in (41) is turned on, the exponentials  $\exp(i\omega t)$  and  $\exp[i\omega(t - \tau)]$  vanish as  $\omega_i \rightarrow -\infty$ , where  $\omega_i$  is the imaginary part of  $\omega$ . The integration path is thus closed in the lower half plane with a semicircle of infinite radius. Since the poles at  $B = 0$  are on the real  $\omega$  axis, exterior to the integration path,  $\tilde{w}(\mathbf{k}, t) = 0$ , as expected for times that precede the forcing.

[77] For  $t > \tau$ , after the forcing is turned off, the exponentials  $\exp(i\omega t)$  and  $\exp[i\omega(t - \tau)]$  vanish as  $\omega_i \rightarrow +\infty$ . The integration path is thus closed in the upper half plane. The poles  $B = 0$  on the real  $\omega$  axis then reside within the integration path. The residue at each pole is obtained by replacing  $B$  in (A5) with its derivative  $B_\omega = 2\omega(k_h^2 + m^2)$  and evaluating the integrand at the respective pole,  $\omega = \pm\sigma(\mathbf{k})$ . The integral (A5) is  $2\pi i$  times the sum of the two residues, resulting in

$$\tilde{w}(\mathbf{k}, t) = \frac{2\pi k_h^2 Q a}{\sigma(k_h^2 + m^2)\tau^2} \frac{\sin(\sigma t) - \sin\sigma(t - \tau)}{a^2 - \sigma^2}, \quad (\text{A6})$$

after taking the limit  $\epsilon \rightarrow 0$ . Using the dispersion relation and, from below (41),  $2\pi = a\tau$ , (A6) reduces to the solution given by Vadas and Fritts [2009, equation (12)]:

$$\tilde{w}(\mathbf{k}, t) = \frac{a^2 \sigma Q}{\tau N^2 (a^2 - \sigma^2)} [\sin(\sigma t) - \sin\sigma(t - \tau)]. \quad (\text{A7})$$

To convert from our notation to that of Vadas-Fritts, let  $a \rightarrow \hat{a}$ ,  $\tau \rightarrow \sigma_b$ ,  $\sigma \rightarrow \omega$ ,  $Q \rightarrow \tilde{F}_z / (2\pi)^3$ , and  $\tilde{w} \rightarrow \tilde{w} / (2\pi)^3$ .

[78] **Acknowledgments.** We thank Sharon Vadas for discussions of her model and the reviewers for their comments. This work was supported by the Office of Naval Research through NRL's base 6.1 work units 9440 (Subgrid-scale Dynamics of Middle and Upper Atmospheres) and 4461 (The Boundary Paradox), and by NASA through its Global Modeling and Analysis Program, contract NNTG06HM191.

## References

- Bühler, O., M. E. McIntyre, and J. F. Scinocca (1999), On shear-generated gravity waves that reach the mesosphere. Part I: Wave generation, *J. Atmos. Sci.*, *56*, 3749–3763.
- Didascalou, D., T. M. Schafer, and F. Weinmann (2000), Ray-density normalization for ray-optical wave propagation modeling in arbitrary shaped tunnels., *IEEE Trans. Antennas Propag.*, *48*(9), 1316–1325.
- Dupont, P., and B. Voisin (1996), Internal waves generated by a translating and oscillating sphere, *Dyn. Atmos. Oceans*, *23*, 289–298.
- Fritts, D. C., and S. L. Vadas (2008), Gravity wave penetration into the thermosphere: Sensitivity to solar cycle variations and mean winds, *Ann. Geophys.*, *26*, 3841–3861.
- Hasha, A., O. Bühler, and J. Scinocca (2008), Gravity wave refraction by three-dimensionally varying winds and the global transport of angular momentum, *J. Atmos. Sci.*, *65*, 2892–2906.
- Hayes, W. D. (1970), Kinematic wave theory, *Proc. R. Soc., Ser. A*, *320*, 209–226.
- Lighthill, J. (1978), *Waves in Fluids*, 504 pp., Cambridge Univ. Press, Cambridge, U. K.
- Lighthill, J. (1996), Internal waves and related initial-value problems, *Dyn. Atmos. Oceans*, *23*, 3–17.
- Shutts, G. (1998), Stationary gravity-wave structure in flows with directional wind shear, *Q. J. R. Meteorol. Soc.*, *124*, 1421–1442.
- Vadas, S. L., and G. Crowley (2010), Sources of the traveling ionospheric disturbances observed by the ionospheric TIDDBIT sounder near Wallops Island on 30 October 2007, *J. Geophys. Res.*, *115*, A07324, doi:10.1029/2009JA015053.
- Vadas, S. L., and D. C. Fritts (2001), Gravity wave radiation and mean responses to local body forces in the atmosphere, *J. Atmos. Sci.*, *58*, 2249–2279.
- Vadas, S. L., and D. C. Fritts (2004), Thermospheric responses to gravity waves arising from mesoscale convective complexes, *J. Atmos. Sol. Terr. Phys.*, *66*, 781–804.
- Vadas, S. L., and D. C. Fritts (2005), Thermospheric responses to gravity waves: Influences of increasing viscosity and thermal diffusivity, *J. Geophys. Res.*, *110*, D15103, doi:10.1029/2004JD005574.
- Vadas, S. L., and D. C. Fritts (2009), Reconstruction of the gravity wave field from convective plumes via ray tracing, *Ann. Geophys.*, *27*, 147–177.
- Vadas, S. L., J. Yue, C.-Y. She, P. A. Stamus, and A. L. Liu (2009), A model study of the effects of winds on concentric rings of gravity waves from a convective plume near Fort Collins on 11 May 2004, *J. Geophys. Res.*, *114*, D06103, doi:10.1029/2008JD010753.
- Voisin, B. (2003), Limit states of internal wave beams, *J. Fluid Mech.*, *496*, 243–293.
- D. Broutman, Computational Physics, Inc., Springfield, VA 22151, USA. (daveb@cpi.com)
- S. D. Eckermann, Space Science Division, Naval Research Laboratory, 4555 Overlook Ave., SW, Washington, DC 20375, USA.